ELSEVIER

Chemical Engineering Journal 112 (2005) 13–22

Chemical Engineering Journal

www.elsevier.com/locate/cej

Synthesis gas production from dry reforming of methane over CeO_2 doped Ni/Al_2O_3: Influence of the doping ceria on the resistance toward carbon formation

N. Laosiripojana [a,*], W. Sutthisripok [b], S. Assabumrungrat [c]

[a] *The Joint Graduate School of Energy and Environment, King Mongkut's University of Technology Thonburi, Bangkok 10140, Thailand*
[b] *Department of Mining and Materials Engineering, Faculty of Engineering, Prince of Songkla University, Songkhla, Thailand*
[c] *Center of Excellence on Catalysis and Catalytic Reaction Engineering, Department of Chemical Engineering, Faculty of Engineering, Chulalongkorn University, Bangkok 10330, Thailand*

Received 17 January 2005; received in revised form 4 June 2005; accepted 9 June 2005

Abstract

Doping of CeO_2 as an additive promoter on Ni/Al_2O_3 was found to improve dry reforming activity for H_2 and CO productions at solid oxide fuel cell (SOFC) operating temperature (800–900 °C). The catalyst provides significantly higher reforming reactivity and resistance toward carbon deposition compared to conventional Ni/Al_2O_3. These enhancements are mainly due to the influence of the redox property of ceria. During dry reforming process, in addition to the reactions on Ni surface, the gas–solid reactions between the gaseous components presented in the system (CH_4, CO_2, CO, H_2O, and H_2) and the lattice oxygen (O_x) on ceria surface also take place. The reactions of adsorbed methane and carbon monoxide (produced during dry reforming process) with the lattice oxygen (O_x) on ceria surface ($CH_4 + O_x \rightarrow CO + H_2 + O_{x-1}$ and $CO + O_x \Leftrightarrow CO_2 + O_{x-1}$) can prevent the formation of carbon species on Ni surface from methane decomposition reaction and Boudard reaction.

In particular, CeO_2 doped Ni/Al_2O_3 with 8% ceria content showed the best reforming activity among those with the ceria content between 0 and 14%. The amount of carbon formation decreased with increasing Ce content. However, Ni was oxidized when more than 10% of ceria was doped. According to the post-XPS measurement, a small formation of Ce_2O_3 was observed after exposure in dry methane reforming conditions with low inlet CH_4/CO_2 ratio (1.0/0.3). The intrinsic reaction kinetics of 8% CeO_2 doped Ni/Al_2O_3 was studied by varying inlet CH_4 and CO_2 concentrations, and by adding H_2 and CO to the system at different temperatures. The dry reforming rate increased with increasing methane partial pressure and the operating temperature. The reaction orders in methane were always closed to 1.0 in all conditions. Carbon dioxide also presented weak positive impact on the methane conversion, whereas adding of carbon monoxide and hydrogen inhibited the reforming rate.

Keywords: Hydrogen; Synthesis gas; Carbon formation; Dry reforming; CeO_2

1. Introduction

Solid oxide fuel cell (SOFC) with an indirect internal reforming operation (IIR), called IIR-SOFC, is expected to be an important technology for energy generation in the near future due to the high efficiency and its low environmental impact. Regarding this operation, the endothermic reforming reaction takes place at the reformer, which is in close thermal contact with the anode side of fuel cell where the exothermic electrochemical reaction takes place (Fig. 1). IIR gives the advantage on eliminating the requirement for a separate fuel reformer and providing good heat transfer between the reformer and the fuel cell. In addition, the reformer part and the anode side for IIR operation can be operated separately. Therefore, the catalyst for reforming reaction at the reformer part and the material for electrochemical reactions at the anode side of fuel cell can be different

* Corresponding author.
E-mail address: navadol_l@jgsee.kmutt.ac.th (N. Laosiripojana).

1385-8947/$ – see front matter © 2005 Elsevier B.V. All rights reserved.
doi:10.1016/j.cej.2005.06.003

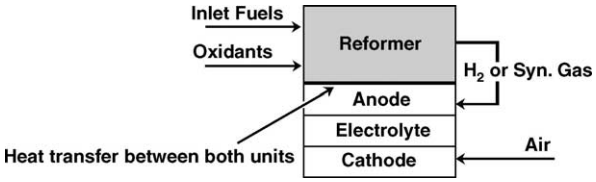

Fig. 1. Diagram of IIR-SOFC operation.

and optimized individually. This operation is expected to simplify the overall system design, making SOFC more attractive and efficient for producing electrical power [1].

The aim of the reformer unit is to reform and maximize the yield of hydrogen production and supply this component to the anode side of SOFC. Theoretically, hydrogen can be produced from several natural hydrocarbon sources including natural gas, bio-ethanol, coal, biomass, and biogas. Biogas consists mainly of methane and carbon dioxide is expected to be the attractive raw material for hydrogen production in the near future due to its economic availability. Due to the rich CO_2 for biogas, carbon dioxide (or dry) reforming reaction would be one of the most suitable processes to convert biogas to hydrogen or synthesis gas (CO and H_2). Compared to the steam reforming, both steam and dry reforming reactions have similar thermodynamic characteristics except that the carbon formation in the dry reforming is more severe than in the steam reforming due to the lower H/C ratio of this reaction [2]. The attractive feature of the dry reforming reaction is the utilisation of CO_2, which is a greenhouse effect gas. In general, the dry reforming reaction (Eq. (1)) is typically accompanied by the simultaneous occurrence of the reverse water-gas shift reaction (RWGS) (Eq. (2)).

$$CH_4 + CO_2 \Leftrightarrow 2CO + 2H_2 \qquad \Delta H = 247\,\text{kJ/mol} \qquad (1)$$

$$CO_2 + H_2 \Leftrightarrow CO + H_2O \qquad \Delta H = 41.1\,\text{kJ/mol} \qquad (2)$$

The hydrogen to carbon monoxide production ratio (H_2/CO ratio) from the dry reforming reaction is always less than 1. Vannice and Bradford [3] presented the apparent activation energies for the consumption of methane and carbon dioxide, as well as the production of carbon monoxide, hydrogen, and water in order to investigate the influence of the RWGS reaction. They observed that the apparent activation energy for hydrogen formation is greater than that for the formation of carbon monoxide, in which supported the influence of the reverse water-gas shift reaction on the reaction mechanism. Sodesawa et al. [4] studied the dry reforming reaction at a stoichiometric feed ratio over several catalysts. They found that the activities of most catalysts deactivated rapidly due to the carbon deposition. Topor et al. [5] suggested that the use of excess carbon dioxide could avoid carbon formation. Chubb et al. [6,7] studied the carbon dioxide reforming using an excess of carbon dioxide with carbon dioxide to methane ratios of 3:1 and 5:1 over Ni/Al_2O_3. They reported that the rate of disintegration is smaller for the higher one. Rostrup-Nielsen and Bak Hansen [8] investigated the activity toward dry reforming over several metals. Their order of reactivity for this reaction was Ru > Rh > Ni ∼ Ir > Pt > Pd, in which similar to their proposed order for steam reforming. They also observed that the replacing of steam with carbon dioxide gave similar activation energies, which indicated a similar rate-determining step in these two reactions. In addition, low levels or no carbon formation was detected from dry reforming over Rh metal at low temperature and CO_2 content [9]. Erdöhelyi et al. [10,11] studied the influence of the catalyst support on the dry reforming of rhodium-based catalyst, and reported that the support had no effect on the activity of Rh. In contrast, Nakamura et al. [12] and Zhang et al. [13] observed that the initial turnover frequency (specific activity) of Rh crystallities was significantly affected by their supports. Zhang et al. [13] also reported that the deactivation of Rh crystallities was strongly dependent on their supports.

In this present study, it is aimed at the development of an alternative catalyst for dry methane reforming reaction, which provided high stability, and activity toward this reaction at such a high temperature (800–900 °C) for later application in IIR-SOFC. According to the economical point of view, Ni/Al_2O_3 was selected as a based catalyst rather than the precious metals. Cerium oxide (CeO_2) was chosen as an additive promoter. This material (called ceria) is an important material for a variety of catalytic reactions involving oxidation of hydrocarbons (e.g. automobile exhaust catalysts). It contains a high concentration of highly mobile oxygen vacancies, which act as local sources or sinks for oxygen involved in reactions taking place on its surface. Nowadays, a potential application of ceria is in solid oxide fuel cells application as a reforming catalyst for in-stack (called indirect internal) reforming of methane, since it is high resistant toward carbon deposition compared to Ni [14]. Recently, the successful test of ceria for the methane steam reforming reaction has been reported [15–17]. Due to the high resistance toward carbon formation, ceria should be a good additive promoter for dry reforming process.

Recently, the use of ceria-based materials as the support and promoter for the catalytic reforming reaction has been reported by several researchers. As the support, it has been reported to be promising support among α-Al_2O_3 [18], γ-Al_2O_3, and γ-Al_2O_3 with alkali metal oxide and rare earth metal oxide [19] and $CaAl_2O_4$ [18–21], while the selected metals were Ni, Pt, or Pd [22–31]. As the promoter, ceria was also reported to be a good promoter for the dry methane reforming at intermediate temperature [32]. Wang and Lu [32] prepared CeO_2 doped Ni/Al_2O_3 by adding CeO_2 on γ-Al_2O_3 powder before impregnated Ni on CeO_2–Al_2O_3 support and tested the dry methane reforming reactivity at 500–800 °C. They found that the doping of CeO_2 significantly improved the resistance of catalyst toward the carbon deposition.

In this work, various amounts of cerium oxide were firstly doped on the surface of Ni/Al_2O_3 in order to determine the suitable doping ratio. The reactivity toward dry reforming and the resistance toward carbon formation over CeO_2 doped Ni/Al_2O_3 was studied and compared to conventional

Ni/Al_2O_3 at the temperature range of 800–900 °C. In addition, the intrinsic kinetics of the dry methane reforming reaction over this catalyst was also studied by varying inlet CH_4, CO_2, and by adding CO and H_2 at different temperatures. The reaction orders in each component and the possible rate isotherm with the fitting parameters were determined. These kinetic informations are important in order to determine the behavior of the catalyst toward this reaction for the large scale or industrial application. By fitting the rate isotherm and parameters in the modeling, the behavior of the whole reformer and the IIR-SOFC system can be predicted.

2. Experimental

2.1. Catalyst preparations

Ni/Al_2O_3 (5 wt.% Ni) was prepared by impregnating α-Al_2O_3 (from Aldrich) with $NiCl_3$ solution at room temperature. This solution was stirred by magnetic stirring (100 rpm) for 6 h, dried overnight in an oven at 110 °C, and calcined in air at 900 °C for 6 h. The catalyst powder was then reduced with 10% H_2/Ar at 700 °C for 6 h. CeO_2 doped Ni/Al_2O_3 was prepared by impregnate different concentration of cerium nitrate ($Ce(NO_3)_3{\cdot}6H_2O$ (99.0%), Fluka) on Ni/Al_2O_3 powder. Similarly, this solution was stirred by magnetic stirring (100 rpm) for 6 h before filtered and washed with deionised water and ethanol to prevent an agglomeration. The sample was dried and calcined in air at 1000 °C for 6 h. It was reduced with 10% H_2/Ar at 700 °C for 6 h before use.

2.2. Apparatus and procedures

In order to investigate the dry reforming and its associated reactions, an experimental reactor system was constructed. The feed gases including the components of interest such as CH_4, CO_2, H_2, or CO were introduced to the reaction section, in which an 8-mm internal diameter and 40-cm length quartz reactor was mounted vertically inside a furnace. The catalyst (50 mg) was loaded in the quartz reactor, which was packed with a small amount of quartz wool to prevent the catalyst from moving. In order to observe the intrinsic reaction kinetics, the methane conversions from dry reforming were always kept below 20% in all experiments.

In the present work, the desired space velocity and suitable catalyst particle size were achieved from several preliminary tests, which were carried out to avoid any limitations by intraparticle diffusion in the experiments. Regarding to these testing, the total flow rate was varied between 20 and 200 $cm^3\,min^{-1}$ under a constant residence time of 5×10^{-4} g min cm^{-3}. When the total flow rate was below 60 $cm^3\,min^{-1}$, the reforming rate increased with increasing the gas flow rate, suggesting that the mass transfer between the bulk gas and the catalyst particles is the rate-determining step. The reforming rate was almost constant in the range where the gas flow rate was higher than 80 $cm^3\,min^{-1}$, indicating that the mass transfer effect is unimportant in this flow rate range. Fig. 2 shows the effect of the total gas flow rate on the reforming rate over 8% CeO_2 doped Ni/Al_2O_3 at different temperatures. The reactions on different average sizes (from 100 to 500 μm) of catalysts were also carried out. It was observed that there were no significant changes in the methane conversion for the catalyst with the particle size between 100 and 200 μm, which indicated that the intraparticle diffusion limitation was negligible in this range of operating conditions. Consequently, the weight of catalyst loading was 50 mg, while the total gas flow was kept constant at 100 $cm^3\,min^{-1}$. The catalyst particle size diameter was between 100 and 200 μm in all experiments.

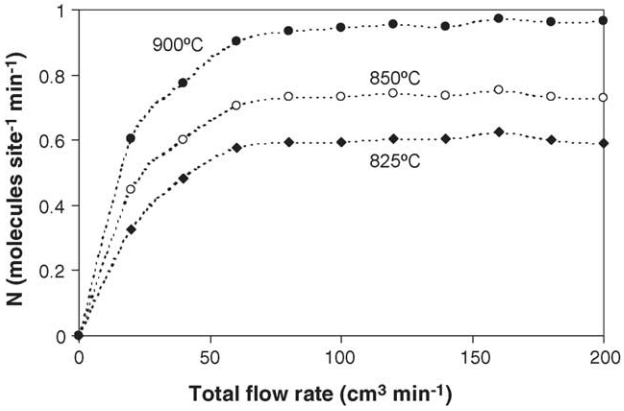

Fig. 2. Effect of the total gas flow rate on the turnover frequencies (*N*) for dry reforming over 8% CeO_2 doped Ni/Al_2O_3 at different temperatures (4 kPa CH_4 and 12 kPa CO_2).

A type-K thermocouple was placed into the annular space between the reactor and the furnace. This thermocouple was mounted on the tubular reactor in close contact with the catalyst bed to minimize the temperature difference between the catalyst bed and the thermocouple. Another type-K thermocouple was inserted in the middle of the quartz tube in order to re-check the possible temperature gradient. The record showed that the maximum temperature fluctuation during the reaction was always ±0.75 °C or less from the temperature specified for the reaction.

After the reactions, the exit gas mixture was transferred via trace-heated lines to the analysis section, which consists of a Porapak Q column Shimadzu 14B gas chromatograph (GC) and a mass spectrometer (MS). The gas chromatography was applied in order to investigate the steady state condition experiments, whereas the mass spectrometer in which the sampling of the exit gas was done by a quartz capillary and differential pumping was used for the transient and carbon formation experiments. In order to study the formation of carbon species on catalyst surface, temperature-programmed oxidation (TPO) was applied by introducing 10% oxygen in helium into the system, after purged with helium. The operating temperature increased from room temperature to 1000 °C by the rate of 10 °C/min. The calibrations of CO and CO_2 productions were performed by injecting a known amount of

these calibration gases from a loop, in an injection valve in the bypass line. The response factors were obtained by dividing the number of moles for each component over the respective areas under peaks. In addition to the TPO method, the amount of carbon deposition was confirmed by the calculation of carbon balance in the system. The amount of carbon deposited on the surface of catalyst would theoretically be equal to the difference between the inlet carbon containing components (CH_4 and CO_2) and the outlet carbon containing components (CO, CO_2, and CH_4). The amount of carbon deposited per gram of catalyst is given by the following equation:

$$C_{\text{deposition}} = \frac{\text{mole}_{\text{carbon (in)}} - \text{mole}_{\text{carbon (out)}}}{m_{\text{catalyst}}} \quad (3)$$

3. Results and discussion

3.1. Catalyst characterizations

After reduction, the catalysts were characterized with several physicochemical methods. The weights content of Ni and Ce loadings were determined by X-ray fluorescence (XRF) analysis. The reducibility and dispersion percentages of nickel were measured from temperature-programmed reduction (TPR) with 5% H_2 in Ar and temperature-programmed desorption (TPD), respectively. The catalyst specific surface areas were obtained from BET measurement. All physicochemical properties of the synthesized catalysts are presented in Table 1. The catalyst specific surface areas slightly increased by the doping of Ce.

3.2. Selection of suitable Ce doping content

After reduction, various Ce contents (from 2 to 14%) doped on Ni/Al_2O_3 were studied in dry reforming at 900 °C. The feed was CH_4/CO_2 in helium with the CH_4/CO_2 ratio of 1.0/0.3. Fig. 3 presents the steady state turnover frequencies (N) for CeO_2 doped Ni/Al_2O_3 with different CeO_2 contents. The turnover frequencies were calculated from the methane conversion following the below equation by assuming that all surface sites accessible by nitrogen adsorption (area per molecule 16.2×10^{-20} m^2 [14]) were active.

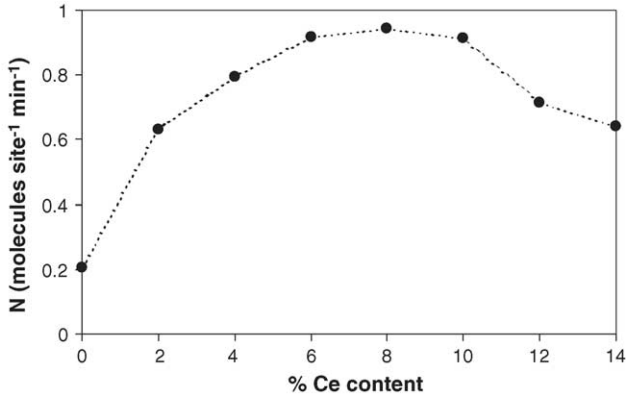

Fig. 3. Effect of Ce doping content on the turnover frequencies (N) for dry reforming (900 °C, 4 kPa CH_4, and 12 kPa CO_2).

$$N = \frac{rN_A A_{N_2}}{m_c S} \quad (4)$$

where r is the reaction rate (moles CH_4 per unit time), N_A the Avagadro's number, A_{N_2} the area occupied by an adsorbed nitrogen molecule (16.2×10^{-20} m^2), m_c the weight of catalyst used (50 mg), and S is the specific surface area of the catalyst. The figure indicates that 8% CeO_2 doping on Ni/Al_2O_3 presents the highest turnover frequencies.

The post-reaction temperature-programmed oxidation experiments were then carried out after a helium purge by introducing of 10% oxygen in helium in order to determine the degree of carbon deposition on the surface of each sample. Table 2 presents the important physicochemical properties of the spent catalysts after exposure in dry reforming conditions for 10 h. According to TPO, the amount of carbon formation decreased with increasing Ce content. No carbon species was observed when the Ce doping content was higher than 8%. The decreasing in the reactivity when more than 10% CeO_2 was doped could be due to the oxidized of Ni, as the reducibility of Ni reduced after exposure in dry reforming for 10 h, regarding to the TPR experiments.

It should also be noted that, at steady state, the main products from this reaction were H_2 and CO with H_2/CO always less than 1, indicating a contribution of the reverse water-

Table 1
Physicochemical properties of the catalysts after reduction at 700 °C

Catalyst	Ni load[a] (wt.%)	Ce load[a] (wt.%)	BET surface area (m^2 g^{-1})	Ni-reducibility[b] (Ni%)	Ni-dispersion[c] (Ni%)
Ni/Al_2O_3	4.91	0.0	40.2	92.1	4.87
2% Ce-Ni/Al_2O_3	4.84	1.87	40.8	93.5	4.54
4% Ce-Ni/Al_2O_3	4.93	4.02	42.7	91.4	5.12
6% Ce-Ni/Al_2O_3	5.01	5.94	46.5	90.6	4.54
8% Ce-Ni/Al_2O_3	4.96	8.03	49.1	91.1	4.65
10% Ce-Ni/Al_2O_3	4.88	9.86	49.8	89.9	4.77
12% Ce-Ni/Al_2O_3	4.93	12.1	50.4	90.3	4.64
14% Ce-Ni/Al_2O_3	4.92	13.9	50.9	91.0	4.20

[a] Measured from X-ray fluorescence analysis.
[b] Measured from temperature-programmed reduction (TPR) with 5% hydrogen.
[c] Measured from temperature-programmed desorption (TPD) of hydrogen after TPR measurement.

Table 2
Methane conversions, H_2/CO production ratio, and physicochemical properties of the catalysts after exposure in dry reforming (4 kPa CH_4 and 12 kPa CO_2) at 900 °C

Catalyst	CH_4 conversions (%) at steady state	H_2/CO ratio	Ni and Ce load[a] (wt.%)	Carbon formation[b] (monolayers)	BET surface ($m^2\ g^{-1}$)	Ni reducibility[c] (Ni%)	Ni dispersion[d] (Ni%)
Ni/Al_2O_3	3.32	0.89	4.89/0.0	3.48	40.0	92.1	4.84
2% Ce-Ni[e]	9.43	0.88	4.86/1.87	3.01	40.8	93.2	4.48
4% Ce-Ni	12.2	0.84	4.96/4.00	1.62	42.0	91.0	5.07
6% Ce-Ni	14.7	0.81	4.97/5.98	0.43	43.9	90.0	4.52
8% Ce-Ni	15.3	0.80	4.98/8.01	∼0	44.4	90.4	4.60
10% Ce-Ni	14.9	0.77	4.83/9.93	∼0	44.7	87.3	4.71
12% Ce-Ni	11.8	0.75	4.87/11.9	∼0	45.1	70.1	4.55
14% Ce-Ni	10.7	0.71	4.94/14.0	∼0	45.6	67.6	4.14

[a] Measured from X-ray fluorescence analysis.
[b] Calculated using CO and CO_2 yields from temperature-programmed oxidation (TPO) with 10% oxygen.
[c] Nickel reducibility (measured from temperature-programmed reduction (TPR) with 5% hydrogen).
[d] Nickel dispersion (measured from temperature-programmed desorption (TPD) after TPR).
[e] CeO_2 dopedNi/Al_2O_3.

gas shift reaction. Small amount of steam was also observed from the reaction. The H_2/CO ratio decreased with increasing Ce doping content indicated the high reactivity toward the reverse water-gas shift reaction of ceria (Table 2). The reactivities toward the reverse water-gas shift reaction for CeO_2 doped Ni/Al_2O_3 (with several Ce contents) and Ni/Al_2O_3 were tested in order to ensure the above explanation by using TPRx in CO_2/H_2/He gas mixture (5 kPa CO_2 and 10 kPa H_2). Fig. 4 shows the activities of all catalysts toward this reaction. Clearly, the activity toward the RWGS reaction over CeO_2 doped Ni/Al_2O_3 with high Ce content was significantly higher than that over Ni/Al_2O_3 at the same operating conditions.

3.3. Reactivity toward dry reforming

Ni/Al_2O_3 and 8% CeO_2 doped Ni/Al_2O_3 were further studied in dry reforming at 900 °C. The feed was CH_4/CO_2 in helium with different CH_4/CO_2 ratios of 1.0/0.3, 1.0/1.0, and 1.0/3.0. The reforming rate was measured as a function of time in order to indicate the stability and the deactivation rate.

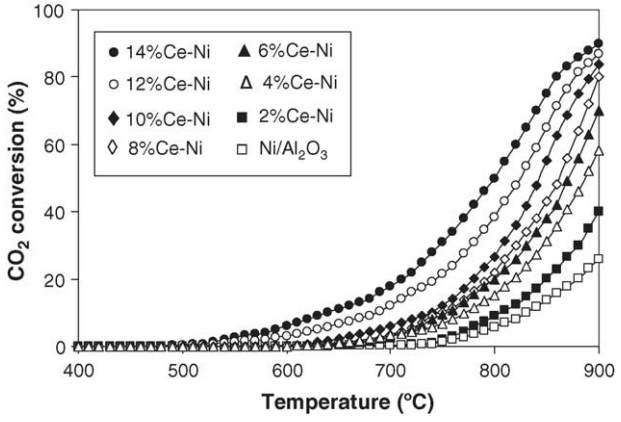

Fig. 4. The activities of Ni/Al_2O_3 and CeO_2 doped Ni/Al_2O_3 (with different Ce contents) toward the reverse water-gas shift reaction using TPRx in CO_2/H_2/He gas mixture (5 kPa CO_2 and 10 kPa H_2).

The variations in turnover frequencies (N) with time at 900 °C for different catalysts and different inlet CH_4/CO_2 ratio are shown in Fig. 5. The significant deactivations were detected for Ni/Al_2O_3 catalyst in all conditions especially at high inlet CH_4/CO_2 ratio, whereas considerable lower deactivations were detected for 8% CeO_2 doped Ni/Al_2O_3. At steady state, the dry reforming over 8% CeO_2 doped Ni/Al_2O_3 with inlet CH_4/CO_2 of 1.0/3.0 showed the best activity. Catalyst stabilities expressed as deactivation percentages are given in Table 3.

The characterization of these spent catalysts by X-ray diffraction (XRD) and X-ray photoelectron spectroscopy (XPS) were then carried out to determine the formation or the changing of chemical states in the spent catalysts, compared to the fresh one after reduction. X-ray diffraction was performed using X-ray defractometer with Cu Kα radiation (λ = 1.54060 Å) and operating parameters of 40 kV and 40 mA. Diffraction patterns were acquired by a step-scanning technique, using a step size ($\Delta 2\theta$) of 0.020°. The XPS spectra were acquired on spectrometer with a hemispherical electron analyser detector, operated in a constant threshold pass energy mode (50 eV), and using a non-monochromatic Al

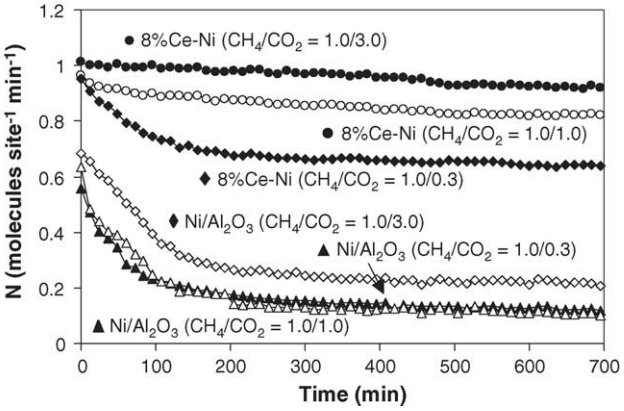

Fig. 5. Dry reforming of methane at 900 °C for several catalysts and various inlet CH_4/CO_2 ratios.

Table 3
Methane conversions, stabilities, and physicochemical properties of the catalysts after exposure in dry reforming conditions at 900 °C for 12 h

Catalyst	CH_4/CO_2 ratio	CH_4 conversions (%) at steady state	Deactivation (%)	Carbon formation[a] (monolayers)	BET after reaction ($m^2\ g^{-1}$)	Ni reducibility[b] (Ni%)
Ni/Al_2O_3	1.0/0.3	1.64	84.2	4.26	40.0	91.0
	1.0/1.0	2.01	78.4	3.97	39.5	93.2
	1.0/3.0	3.32	69.9	3.48	40.0	92.1
8% Ce-Ni[c]	1.0/0.3	10.6	33.1	0.85	44.0	90.0
	1.0/1.0	13.6	14.8	0.34	44.5	89.3
	1.0/3.0	15.3	9.08	~0	44.4	90.4

[a] Calculated using CO and CO_2 yields from temperature-programmed oxidation (TPO) with 10% oxygen.
[b] Nickel reducibility (measured from temperature-programmed reduction (TPR) with 5% hydrogen).
[c] CeO_2 doped Ni/Al_2O_3.

Kα (1.4866 eV) radiation source, which operated at 12 kV and 20 mA. Fig. 6 presents the XRD patterns of the spent and fresh Ni/Al_2O_3 and CeO_2 doped Ni/Al_2O_3. From the XRD results, Ni and $NiAl_2O_4$ reflectance were found in both Ni/Al_2O_3 and CeO_2 doped Ni/Al_2O_3. It is clearly seen that the intensities of $NiAl_2O_4$ peaks for CeO_2 doped Ni/Al_2O_3 were lower than that for Ni/Al_2O_3. This implies that the interaction between NiO and Al_2O_3 was prevented by the doping of CeO_2. A significant carbon peak was observed for the spent Ni/Al_2O_3, indicated the high formation of carbon species on the catalyst surface, whereas a smaller peak of carbon was detect for the spent CeO_2 doped Ni/Al_2O_3.

Table 4 presents the Ce^{3+}/Ce^{4+} ratio for CeO_2 doped Ni/Al_2O_3 before and after exposure in dry methane reforming conditions, determined from XPS. It is seen that no Ce^{3+} (Ce_2O_3) formation was observed for the fresh CeO_2 doped Ni/Al_2O_3 after reduction. Regarding the spent CeO_2 doped Ni/Al_2O_3, no Ce^{3+} formation was detect after exposure in dry methane reforming with the inlet CH_4/CO_2 ratios of 1.0/3.0 and 1.0/1.0, however, a small formation of Ce_2O_3 was observed over CeO_2 doped Ni/Al_2O_3 catalyst after exposure in dry methane reforming with the inlet CH_4/CO_2 ratio of 1.0/0.3. This Ce_2O_3 formation is obviously due to the remaining non-oxidation CeO_2, which will be explained at the end of this section.

Table 4
Ce^{3+}/Ce^{4+} ratio observed from the XPS measurement over CeO_2 doped Ni/Al_2O_3 after reduction and after exposure in dry methane reforming conditions

	Ce^{3+}/Ce^{4+} ratio
After reduction	0
After exposure in dry methane reforming; with CH_4/CO_2 of	
1.0/3.0	0
1.0/1.0	0
1.0/0.3	0.21

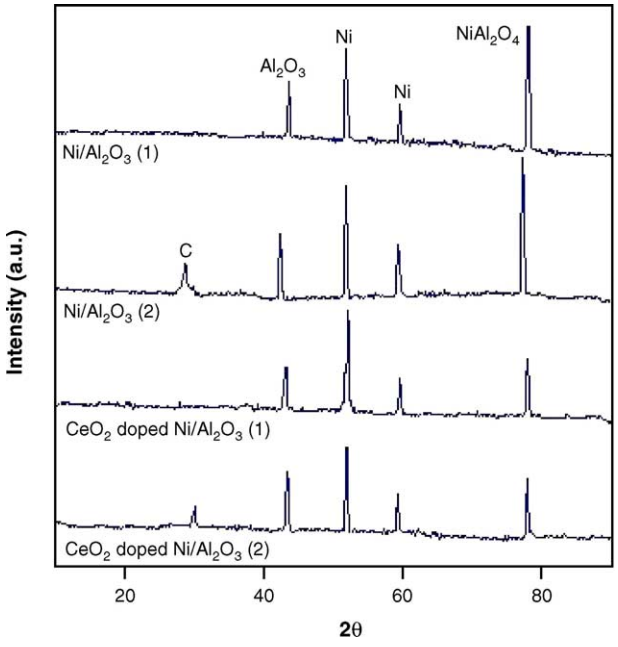

Fig. 6. XRD patterns of the catalysts after reduction (1) and after exposure in dry methane reforming at 900 °C with the inlet CH_4/CO_2 of 1.0/1.0 (2).

The post-reaction temperature-programmed oxidation experiments were then carried out after a helium purge by introducing of 10% oxygen in helium in order to determine whether the observed deactivation is due to the carbon formation. From the TPO results shown in Fig. 7, the huge peaks of carbon dioxide and carbon monoxide were observed for Ni/Al_2O_3 at 600 °C, while smaller peaks of both components were detected for 8% CeO_2 doped Ni/Al_2O_3. The amount of carbon formations on the surface of these catalysts with

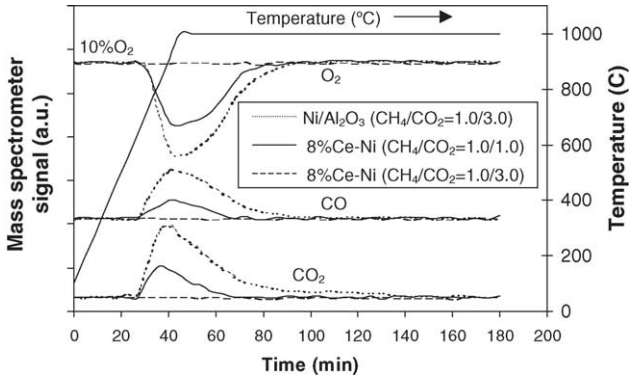

Fig. 7. Temperature-programmed oxidation (TPO) of Ni/Al_2O_3 and 8% CeO_2 doped Ni/Al_2O_3 (10 kPa O_2) after exposure in dry reforming conditions for 10 h.

different inlet CH_4/CO_2 ratios were determined by measuring the CO and CO_2 yields from the TPO results (using Microcal Origin Software). Using a value of 0.026 nm^2 for the area occupied by a carbon atom in a surface monolayer of the basal plane in graphite [17], the quantities of carbon deposited over Ni/Al_2O_3 were observed to be approximately 4.26, 3.97, and 3.48 monolayers, while those over 8% CeO_2 doped Ni/Al_2O_3 were 0.85, 0.34, and ~0 monolayers for the inlet CH_4/CO_2 ratios of 1.0/0.3, 1.0/1.0, and 1.0/3.0, respectively. The total amounts of carbon deposited were ensured by the calculation of carbon balance in the system. Regarding to the calculation for the inlet CH_4/CO_2 ratios of 1.0/0.3, 1.0/1.0, and 1.0/3.0, the moles of carbon deposited per gram of 8% CeO_2 doped Ni/Al_2O_3 were 1.34, 0.49, and ~0 mmol g^{-1}. By the same assumption for the area occupied by a carbon atom [17], these values are equal to 0.87, 0.32, and 0 monolayers, respectively, which is in good agreement with the values observed from the TPO method described above. The results clearly indicated the strong resistance toward carbon formation for 8% CeO_2 doped Ni/Al_2O_3 compared to Ni/Al_2O_3. The BET measurements, as presented in Table 3, indicated that deactivations of 8% CeO_2 doped Ni/Al_2O_3 are also due to the slight sintering of CeO_2. Several researchers also reported the high thermal sintering rate of ceria-based materials at high operating temperature [15,16].

The improvement of dry reforming reactivity and resistance toward carbon formation for CeO_2 doped Ni/Al_2O_3 could be mainly due to the redox property of ceria. During the dry reforming, in addition to the reactions on Ni surface, the solid–gas reaction between CeO_2 and CH_4 also produces synthesis gas with a H_2/CO ratio of two, while the reduced ceria, CeO_{2-x}, can react with CO_2 to produce CO [33–35]. This solid–gas mechanism involves the reactions between methane and/or an intermediate surface hydrocarbon species with the lattice oxygen (O_x) at CeO_2 surface, as illustrated schematically below [36].

$$CH_4 + 2S \Leftrightarrow CH_3{-}S + H{-}S \quad (5)$$

$$CH_3{-}S + S \Leftrightarrow CH_2{-}S + H{-}S \quad (6)$$

$$CH_2{-}S + S \Leftrightarrow CH{-}S + H{-}S \quad (7)$$

$$CH{-}S + S \Leftrightarrow C{-}S + H{-}S \quad (8)$$

$$C{-}S + O_x \Leftrightarrow CO + O_{x-1} + S \quad (9)$$

$$2H{-}S \Leftrightarrow H_2 + 2S \quad (10)$$

During the dry reforming, methane is adsorbed on either a unique site (S) or the lattice oxygen (O_x), whereas CO_2 can react with the reduced site of ceria, O_{x-1}. The steady state reforming rate is mainly due to the continuous supply of the oxygen source by CO_2 (Eq. (11)). Therefore, the Ce_2O_3 formation observed by XPS measurement in Table 4 over spent CeO_2 doped Ni/Al_2O_3 after exposure in dry methane reforming with high inlet CH_4/CO_2 ratio is due to the insufficient supply of inlet CO_2.

$$CO_2 + O_{x-1} \Leftrightarrow O_x + CO \quad (11)$$

Regarding the possible carbon formation during the reforming processes, the following reactions are the most probable reactions that could lead to carbon formation:

$$2CO \Leftrightarrow CO_2 + C \quad (12)$$

$$CH_4 \Leftrightarrow 2H_2 + C \quad (13)$$

$$CO + H_2 \Leftrightarrow H_2O + C \quad (14)$$

$$CO_2 + 2H_2 \Leftrightarrow 2H_2O + C \quad (15)$$

At low temperature, reactions (14) and (15) are favorable, while reaction (12) is thermodynamically unflavored [37]. The Boudard reaction (Eq. (12)) and the decomposition of methane (Eq. (13)) are the major pathways for carbon formation at such a high temperature as they show the largest change in Gibbs energy [38]. According to the range of temperature in this study, 800–900 °C, carbon formation would be formed via the decomposition of methane and Boudard reactions. By doping CeO_2 as the promoter, both reactions (Eqs. (12) and (13)) could be inhibited by the gas–solid reactions between methane and carbon monoxide with the lattice oxygen (O_x) at CeO_2 surface forming hydrogen and carbon dioxide, which is thermodynamically unflavored to form carbon species.

3.4. Effects of temperature and inlet components

The inlet methane partial pressure was varied from 1 to 4 kPa, while inlet carbon dioxide partial pressure was kept constant at 12 kPa. The operating temperature range was 825–900 °C. Fig. 8 illustrates the influence of the inlet methane partial pressure on the turnover frequencies (N) for dry reforming over 8% CeO_2 doped Ni/Al_2O_3 at different operating temperatures. The activities of catalyst increased with increasing inlet methane partial pressure as well as operating temperature. Fig. 9 shows an Arrhenius-type plot

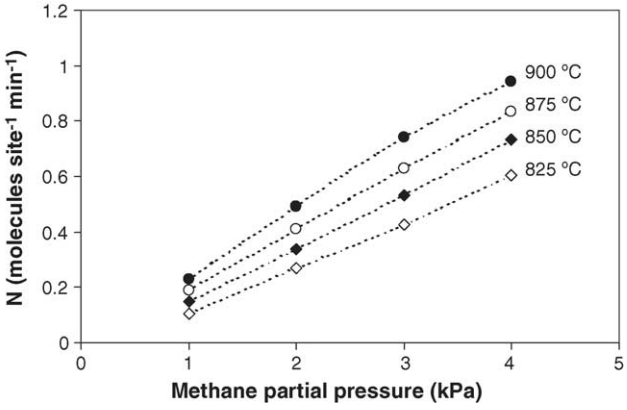

Fig. 8. Effect of methane partial pressure on the turnover frequencies (N) for dry reforming over 8% CeO_2 doped Ni/Al_2O_3 at different temperatures (12 kPa inlet CO_2).

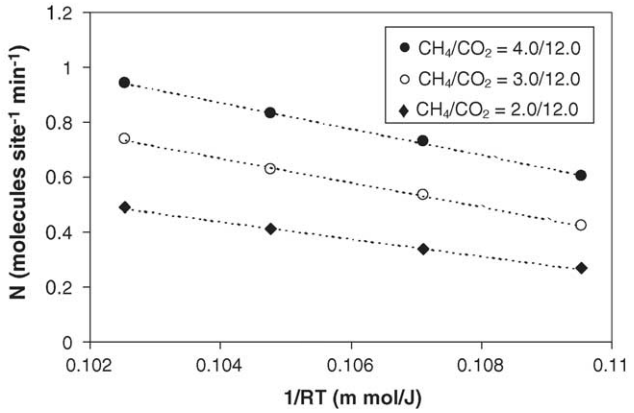

Fig. 9. Arrhenius plot of turnover frequencies (N) for dry reforming of methane over 8% CeO_2 doped Ni/Al_2O_3 with different inlet methane/carbon dioxide ratio.

for dry reforming over CeO_2 doped Ni/Al_2O_3 with various methane/carbon dioxide ratios over the temperature range 825–900 °C. The corresponding activation energy observed for this catalyst is 178 ± 9 kJ/mol, slightly depending on the gas composition.

The reaction order in methane (n) for CeO_2 doped Ni/Al_2O_3 was observed to be 0.96–1.04, and seemed to be essentially independent of the operating temperature and other inlet compositions in the range of conditions studied. These values n were obtained experimentally by plotting $\ln(-r_{CH_4})$ versus $\ln(P_{CH_4})$ according to the equation below.

$$\ln(-r_{CH_4}) = \ln(k) + n\ \ln(P_{CH_4}) \quad (16)$$

where $-r_{CH_4}$ is the dry reforming rate (mol kg_{cat}^{-1} h^{-1}), while P_{CH_4} the methane partial pressure. k is the apparent reaction rate constant and n is the reaction order in methane. The reaction orders in other components (CO_2, H_2, and CO) were achieved using the same approach by varying the inlet partial pressure of the component of interest and keeping other inlet component partial pressures constant.

In order to investigate the influence of CO_2 on the dry reforming rate, several inlet carbon dioxide partial pressures, from 9 to 12 kPa, were introduced to the feed with constant methane partial pressure (3 kPa). Carbon dioxide presented slight positive effect on the dry reforming rate as shown in Fig. 10. The reaction order in carbon dioxide was observed to be a positive value between 0.44 and 0.54, and seemed to be independent of the operating temperature for the range of conditions studied. At 900 °C, the proportion of H_2/CO in the products reduced from 0.80 to 0.67 as the CO_2/CH_4 ratio was increased from 3.0 to 12.0 (Fig. 11). This is as expected from an increasing contribution from the reverse water-gas shift (RWGS) reaction.

The dry reforming in the presences of carbon monoxide and hydrogen were then investigated by adding either carbon monoxide or hydrogen to the feed gas at several operating temperatures. The results show that the reforming rates are also dependent on both carbon monoxide and hydrogen

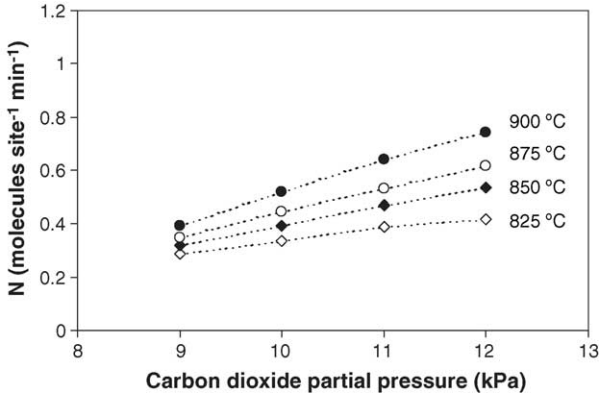

Fig. 10. Effect of carbon dioxide partial pressure on the turnover frequencies (N) for dry reforming over 8% CeO_2 doped Ni/Al_2O_3 at different temperatures (3 kPa CH_4).

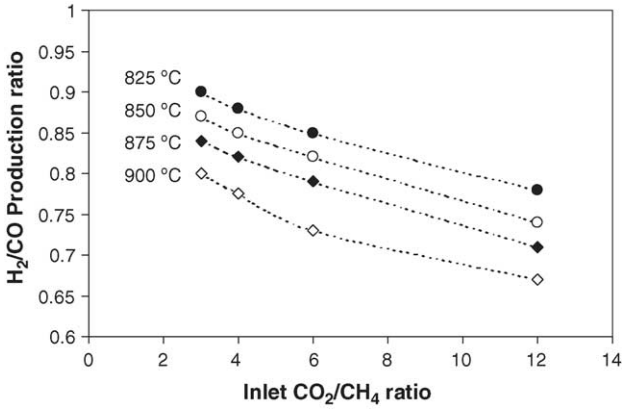

Fig. 11. Influence of inlet carbon dioxide/methane ratio on H_2/CO production ratio from dry reforming of methane over 8% CeO_2 doped Ni/Al_2O_3 at different temperatures (12 kPa CO_2).

concentrations. Unlike CH_4 and CO_2, both components inhibited the dry reforming rate as shown in Figs. 12 and 13. The reaction order in carbon monoxide was in the range of −0.42 to −0.37, while the reaction order in hydrogen was between −0.55 and −0.45 in the range of conditions studied.

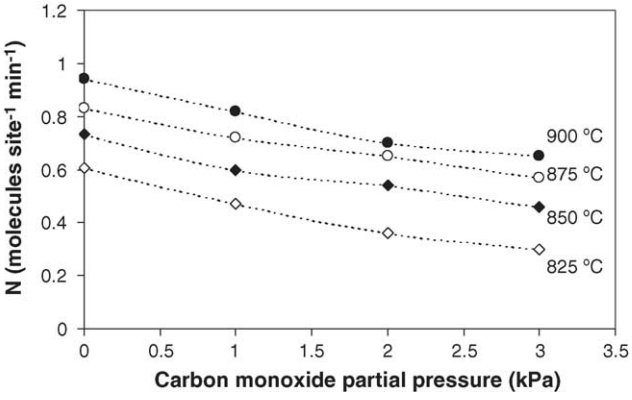

Fig. 12. Effect of carbon monoxide partial pressure on the turnover frequencies (N) for dry reforming of methane over 8% CeO_2 doped Ni/Al_2O_3 at different temperatures (4 kPa CH_4 and 12 kPa CO_2).

Table 5
Reaction orders for the components of interest (CH_4, CO_2, CO, and H_2) from dry reforming over 8% CeO_2 doped Ni/Al_2O_3 at different operating conditions

Components of interest	Temperature (°C)	Other inlet compositions	Reaction order for components of interest
Methane (1–4 kPa)	825	12 kPa CO_2	1.00
	850	12 kPa CO_2	0.97
	900	12 kPa CO_2	0.98
	850	15 kPa CO_2	1.01
	850	17 kPa CO_2	0.99
	825–900	12 kPa CO_2/1 kPa H_2	1.01 ± 0.03
	825–900	12 kPa CO_2/3 kPa H_2	0.98 ± 0.01
	825–900	12 kPa CO_2/1 kPa CO	0.99 ± 0.03
Carbon dioxide (9–12 kPa)	825	3 kPa CH_4	0.44
	850	3 kPa CH_4	0.54
	900	3 kPa CH_4	0.50
	850	3 kPa CH_4/3 kPa H_2	0.48
Hydrogen (1–3 kPa)	825–900	3 kPa CH_4/12 kPa CO_2	-0.49 ± 0.04
	825–850	1 kPa CH_4/12 kPa CO_2	-0.48 ± 0.03
	825–850	3 kPa CH_4/15 kPa CO_2	-0.52 ± 0.03
Carbon monoxide (1–3 kPa)	825–900	3 kPa CH_4/12 kPa CO_2	-0.40 ± 0.01
	825–850	3 kPa CH_4/15 kPa CO_2	-0.38 ± 0.01
	825–850	3 kPa CH_4/17 kPa CO_2	-0.40 ± 0.02

Table 5 presents the summary of observed reaction orders in each component (CH_4, CO_2, CO, and H_2) for CeO_2 doped Ni/Al_2O_3 at different inlet conditions.

Regarding to the above experiments, the experimental data can be fitted well to a simple relative rate coefficient, in which captures the essential features.

$$-r_{CH_4} = \frac{k(T)(P_{CH_4})^n(P_{CO_2})^m}{1 + K_1(T)P_{CO}^a + K_2(T)P_{H_2}^b} \quad (17)$$

where P_i is the partial pressure of chemical component i. The positive effects of methane and carbon dioxide on the dry reforming rate were a consequence of the presence of the $k(T)(P_{CH_4})^n(P_{CO_2})^m$ term, whereas negative effects of carbon monoxide and hydrogen were a consequence of the $K_1(T)P_{CO}^a$ and $K_2(T)P_{H_2}^b$ terms in the denominator. According to the fitting, when n, m, a, and b were taken as 1.0, 0.5, 0.4, and 0.5, a good fit to the data was observed in the range of conditions studied. $k(T)$ increased from 649.0 mol kg^{-1} h^{-1} atm$^{-1.5}$ at 825 °C to 954.3 mol kg^{-1} h^{-1} atm$^{-1.15}$ at 900 °C, while $K_1(T)$ and $K_2(T)$, also temperature dependent parameters, were in the range of 1.68–4.43 atm$^{-0.4}$ and 0.93–3.94 atm$^{-0.5}$, respectively. It should be noted that the apparent activation energy for this reaction, which were achieved by the Arrhenius plots, was approximately 150 kJ/mol.

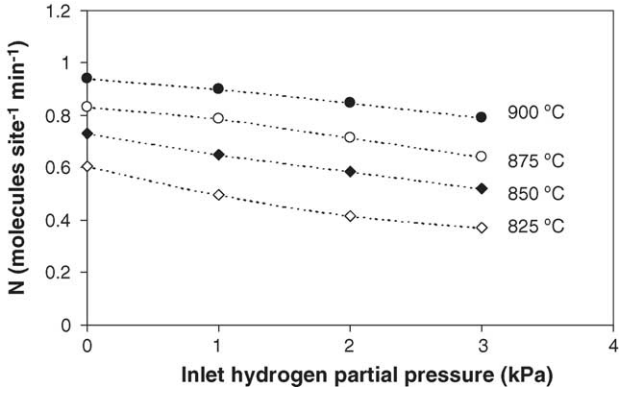

Fig. 13. Effect of hydrogen partial pressure on the turnover frequencies (N) for dry reforming of methane over 8% CeO_2 doped Ni/Al_2O_3 at different temperatures (4 kPa CH_4 and 12 kPa CO_2).

4. Conclusion

8% CeO_2 doped Ni/Al_2O_3 is a good candidate catalyst for the dry reforming of methane due to the high resistance toward the deactivation from carbon formation. During dry reforming process, the gas–solid reaction on ceria surface takes place simultaneously with the reactions on the surface of Ni, in which reduces the degree of carbon deposition on catalyst surface from methane decomposition and Boudard reactions. However, it should also be noted that the doping of too high ceria content results in the oxidation of Ni, which could reduce the reforming reactivity.

The intrinsic kinetic reaction of 8% CeO_2 doped Ni/Al_2O_3 was studied in the conditions where the intraparticle diffusion limitation was negligible. The dry reforming rate increased with increasing methane and carbon dioxide partial pressures as well as the operating temperature. In contrast, the methane conversion was inhibited when hydrogen and carbon monoxide were added to the system during dry reforming process. It can be concluded from the present work that CeO_2 doped Ni/Al_2O_3 seems to be a promise catalyst for the indirect internal reforming solid oxide fuel cells (IIR-SOFC) operation.

Acknowledgement

The financial support from The Thailand Research Fund (TRF) throughout this project is gratefully acknowledged.

References

[1] P. Aguiar, D. Chadwick, L. Kershenbaum, Chem. Eng. Sci. 57 (2002) 1665.
[2] J.H. Edwards, A.M. Maitra, Fuel Process. Technol. 42 (1995) 269.
[3] M.A. Vannice, M.C.J. Bradford, Appl. Catal. A: Gen. 142 (1) (1996) 97–122.
[4] T. Sodesawa, A. Dobashi, F. Nozaki, React. Kinet. Catal. Lett. 12 (1979) 107.
[5] L. Topor, L. Bejan, E. Ivana, N. Georgescu, Rev. Chim. Bucharest 30 (1979) 539.
[6] T.A. Chubb, Sol. Energy 24 (1980) 341.
[7] T.A. Chubb, J.H. McCrary, G.E. McCrary, J.J. Nemecek, D.E. Simmons, Proc. Meet. Am. Sect. Int. Sol. Eng. Soc. 4 (1981) 166.
[8] J.R. Rostrup-Nielsen, J.H. Bak Hansen, J. Catal. 144 (1993) 38.
[9] P. Gronchi, C. Mazzocchia, E. Tempesti, R. Del Rosso, in: G. Centi, et al. (Eds.), Enviromental Catalysis, SCI Publication, Roma, 1995, p. 627.
[10] A. Erdöhelyi, J. Cserényi, F. Solymosi, J. Catal. 141 (1993) 287.
[11] A. Erdöhelyi, J. Cserényi, E. Rapp, F. Solymosi, Appl. Catal. A: Gen. 108 (1994) 205.
[12] J. Nakamura, K. Aikawa, K. Sato, T. Uchijima, Catal. Lett. 25 (1994) 265.
[13] Z.L. Zhang, V.A. Tsipouriari, A.M. Efstathiou, X.E. Verykios, J. Catal. 158 (1996) 51.
[14] E. Ramírez-Cabrera, A. Atkinson, D. Chadwick, Appl. Catal. B 47 (2004) 127–131.
[15] E. Ramírez-Cabrera, N. Laosiripojana, A. Atkinson, D. Chadwick, Catal. Today 78 (2003) 433–438.
[16] N. Laosiripojana, Reaction engineering of indirect internal steam reforming of methane for application in solid oxide fuel cells, Ph.D. Thesis, University of London, England, 2003.
[17] E. Ramirez, A. Atkinson, D. Chadwick, Appl. Catal. B 36 (2002) 193–206.
[18] X. Wang, R.J. Gorte, Appl. Catal. A 224 (2002) 209–218.
[19] H.S. Roh, K.W. Jun, W.S. Dong, J.S. Chang, S.E. Park, Y.I. Joe, J. Mol. Catal. A 181 (2002) 137–142.
[20] Q. Miao, G. Xiong, S. Sheng, W. Cui, L. Xu, X. Guo, Appl. Catal. A 154 (1987) 17–27.
[21] A.A. Lemonidou, M.A. Goula, I.A. Vasalos, Catal. Today 46 (1987) 175–183.
[22] W.S. Dong, H.S. Roh, K.W. Jun, S.E. Park, Y.S. Oh, Appl. Catal. A 226 (2002) 63–72.
[23] M. Mamak, N. Coombs, G. Ozin, Adv. Mater. 12 (2000) 198–202.
[24] M. Mamak, N. Coombs, G. Ozin, J. Am. Chem. Soc. 122 (2000) 8932.
[25] M. Mamak, N. Coombs, G.A. Ozin, Chem. Mater. 13 (2001) 3564.
[26] P. Bera, S. Mitra, S. Sampath, M.S. Hegde, Chem. Commun. (2001) 927.
[27] A. Martinez-Arias, J.M. Coronado, R. Cataluna, J.C. Conesa, J.C. Soria, J. Phys. Chem. B 102 (1998) 4357.
[28] D. Skarmoutsos, F. Tietz, P. Nikolopoulos, Fuel Cells 1 (2001) 243.
[29] T. Takeguchi, S.N. Furukawa, M. Inoue, J. Catal. 202 (2001) 14.
[30] J. Sfeir, P.A. Philippe, P. Moseki, N. Xanthopoulos, R. Vasquez, J.M. Hans, V.H. Jan, K.R. Thampi, J. Catal. 202 (2001) 229.
[31] N. Kiratzis, P. Holtappels, C.E. Hatchwell, M. Mogensen, J.T.S. Irvine, Fuel Cells 1 (2001) 211.
[32] S. Wang, G.Q. Lu, Appl. Catal. B 19 (1998) 267.
[33] K. Otsuka, T. Ushiyama, I. Yamanaka, Chem. Lett. (1993) 1517.
[34] K. Otsuka, M. Hatano, A. Morikawa, J. Catal. 79 (1983) 493.
[35] K. Otsuka, M. Hatano, A. Morikawa, Inorg. Chim. Acta 109 (1985) 193.
[36] N. Laosiripojana, S. Assabumrungrat, Appl. Catal. B 60 (2005) 109–118.
[37] Y. Lwin, W.R.W. Daud, A.B. Mohamad, Z. Yaakob, Int. J. Hydrogen Energy 25 (1) (2000) 47–53.
[38] J.N. Amor, Appl. Catal. A 176 (1999) 159–176.